Journal of Hydraulic Research Vol. 54, No. 2 (2016), pp. 172–184
http://dx.doi.org/10.1080/00221686.2015.1132275

Research paper

Local scour at submerged weirs in sand-bed channels

DAWEI GUAN, Lecturer, *College of Harbour, Coastal and Offshore Engineering, Hohai University, Nanjing, PR China*
Email: david.guan@hhu.edu.cn (author for correspondence)

BRUCE MELVILLE (IAHR Member), Professor, *Department of Civil and Environmental Engineering, The University of Auckland, Auckland, New Zealand*
Email: b.melville@auckland.ac.nz

HEIDE FRIEDRICH (IAHR Member), Senior Lecturer, *Department of Civil and Environmental Engineering, The University of Auckland, Auckland, New Zealand*
Email: h.friedrich@auckland.ac.nz

ABSTRACT
Submerged weirs are river training structures that are used for raising upstream water level, bed stabilization and reducing flow velocity. This paper presents an experimental study of local scour at submerged weirs in sand-bed channels. Two types of tests (coarse sand tests and fine sand tests) were conducted to investigate the effects of sediment size and tailwater depth on scouring at submerged weirs. The flow regimes over the weir are found to be independent of the sediment size, and the transition flow regime boundary can be expressed as a function of upstream Froude number and the ratio of weir height to tailwater depth. New equations, including the effects of sediment size, tailwater depth, flow intensity, and weir height, are proposed for prediction of equilibrium scour depths both upstream and downstream of the submerged weir. A new design method is given for estimating the maximum scour depths at the weir.

Keywords: Bedform; clear-water scour; flow regime; live-bed condition; scour; submerged weir

1 Introduction

Local scouring frequently occurs at hydraulic structures in sand-bed channels as a result of flow disturbance. Depending on the sediment transport conditions in the approach flow, the local scour is classified as clear-water scour and live-bed scour.

Weirs (or sills, as they are alternatively termed) are river training structures, which span the full width of the channel, for limiting channel incision, bed stabilization, reducing flow velocity and raising upstream water level (Chen, Shao, & Zhang, 2005; Guan, Melville, & Friedrich, 2014). To date, scouring downstream of weirs has been extensively studied and many empirical equations have been developed (Ben Meftah & Mossa, 2006; Bormann & Julien, 1991; D'Agostino & Ferro, 2004; Gaudio, Marion, & Bovolin, 2000; Guan, Melville, & Friedrich, 2015; Lenzi, Marion, & Comiti, 2003a, 2003b; Lenzi, Marion, Comiti, & Gaudio, 2002; Lu, Hong, Chang, & Lu, 2012; Marion, Lenzi, & Comiti, 2004; Marion, Tregnaghi, & Tait, 2006; Pagliara & Kurdistani, 2013; Scurlock, Thornton, & Abt, 2012). D'Agostino and Ferro (2004) developed an approach for predicting the scour depth downstream of grade-control weirs. In their research the scour depths were caused by free over-fall jets. Marion et al. (2006) evaluated the effect of upstream sediment supply on the scour hole dimensions downstream of a series of bed sills. Scurlock et al. (2012) and Pagliara and Kurdistani (2013) experimentally studied scour at three-dimensional weirs in clear water scour conditions. However, due to the challenging operability of the experiments, only a few of the equations include the effect of the upstream sediment supply (Bhuiyan, Hey, & Wormleaton, 2009; Guan et al., 2015; Marion et al., 2006). Also, most of the existing equations are developed for weirs in unsubmerged or partially submerged conditions.

The turbulence structures and flow patterns in a scour hole downstream of a submerged weir have been presented in Guan et al. (2014). The experiments in their study were confined to clear water scour conditions. The turbulence structures ahead

Received 9 December 2014; accepted 9 December 2015/Open for discussion until 31 October 2016.

ISSN 0022-1686 print/ISSN 1814-2079 online
http://www.tandfonline.com

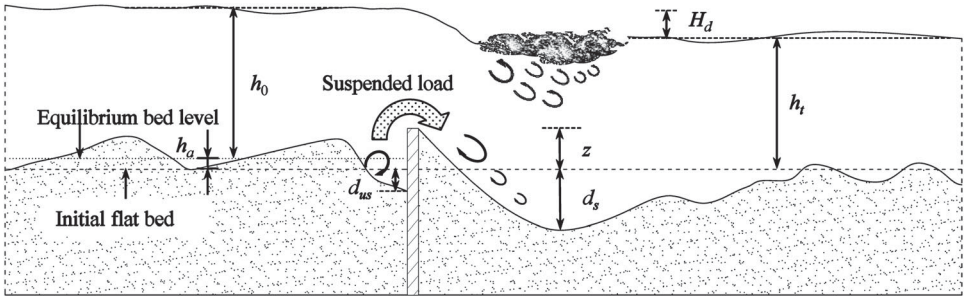

Figure 1 Definition sketch of live-bed scour at a submerged weir, after Guan et al. (2015)

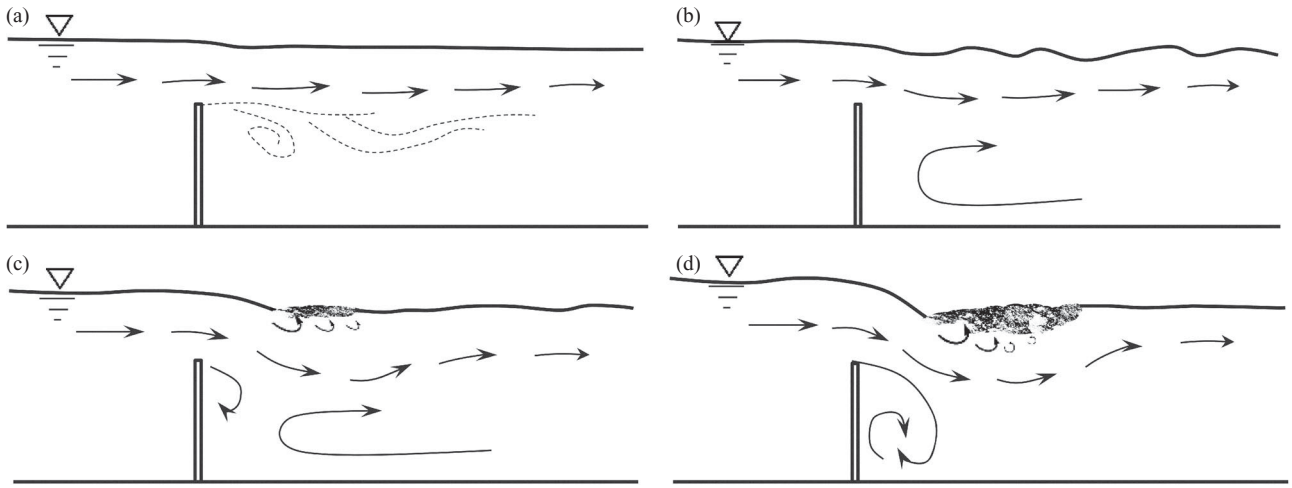

Figure 2 Flow regimes and scour profiles at a submerged weir: (a) SFR (surface jet); (b) SFR (surface wave); (c) TR; (d) IJR, after Guan et al. (2015)

of the recirculation zone were found to govern the dimensions of the scour hole. Guan et al. (2015) first investigated the bedform effect on scour at rectangular submerged weirs with a uniform coarse sand. A sketch of scouring at a submerged weir under live-bed scour conditions is shown in Fig. 1, in which h_a = average aggradation height; h_0 = average approach flow depth; h_t = tailwater depth; H_d = water level difference across the weir; z = weir height; d_{us} = scour depth upstream of the weir; and d_s = scour depth downstream of the weir. It is found that the scour process occurs both upstream and downstream of the weir. A scour-and-fill process and aggradation occur upstream of the weir, and the scour depth is dependent on the geometry of propagating bedforms. Downstream of the weir, the scour depth is found to be strongly influenced by weir height, flow intensity and the flow regimes passing over the weir. However, the results from Guan et al. (2015) did not reveal the sediment size effect and the tailwater depth effect on scouring at submerged weirs.

Although many studies on flow regimes over weir-like structures can be found in the literature (Adduce & La Rocca, 2006; Adduce & Sciortino, 2006; Azimi, Rajaratnam, & Zhu, 2014; Comiti, Cadol, & Wohl, 2009; Comiti & Lenzi, 2006; Fritz & Hager, 1998; Guan et al., 2015; Kabiri-Samani, Ansari, & Borghei, 2010; Wu & Rajaratnam, 1996, 1998), among them only a few focus on flow regimes over submerged weirs (Fritz & Hager, 1998; Guan et al., 2015; Wu & Rajaratnam, 1996). According to Wu and Rajaratnam (1996), the flow regimes passing over a submerged weir can be generally classified as: (1) surface flow regime (SFR), which includes surface flow and surface wave regimes; (2) transition regime (TR); and (3) impinging jet regime (IJR). The flow regimes and the corresponding general scour profiles at the weir are sketched in Fig. 2. For the SFR, the flow remains as a surface jet downstream of the submerged weir, and the scour hole downstream of the weir is caused by the increasing jet thickness and turbulence mixing with the tailwater. For the IJR, the scour hole downstream of the weir is induced by the direct impact of the plunging jet over the weir. Guan et al. (2015) found that the TR occurs at a parameter value $\alpha = (U_0/U_c)(z/h_t)^{0.2} \approx 1.45$ (where U_0 is average approach flow velocity, U_c is critical approach flow velocity, U_0/U_c is flow intensity, and z/h_t is the ratio between weir height and tailwater depth) from their live-bed scour tests. Although the parameter is simple and easy to use, its value may change when the critical average velocity U_c changes as a result of using another sediment size.

The key objectives of this study are (1) to understand the effects of sediment size and tailwater on scouring at submerged weirs; (2) to develop a new method, which is independent of

sediment size, of determining the TR over a submerged weir; and (3) to develop a more comprehensive empirical prediction method for the scour depths at submerged weirs.

2 Experimental set-up and programme

Experiments were carried out in the Hydraulic Laboratory at the University of Auckland. Two types of experiments were undertaken, using two uniform sands with d_{50} equal to 0.26 mm and 0.85 mm, respectively. The characteristics of the sediments are summarized in Table 1, in which σ_g is standard deviation of sediment size and Δ is relative submerged particle density. The critical shear velocity, u_{*c}, is determined from the Shields curve for the respective sediment size (Melville, 1997). A glass-sided recirculating flume, which is 12 m long, 0.44 m wide, and 0.58 m deep, was used. The flume has a main water pump and a sand pump. The sand pump speed was set at a constant value with an adequate capacity for recirculating sediment. The water pump, used for circulating water, is controlled by a variable electronic unit. At the upstream inlet to the open channel section, sediment and water are mixed in a mixing chamber and enter the open channel via a honeycomb flow straightener. At the end of the flume, bed-load sediment is trapped in a separate hopper-like sump and pumped to the inlet by the sand pump. The flume slope was adjusted using a built-in jack. The slope of the flume was calculated from the lifting height of the jack and the distance between the jack and the pivot point. The submerged weirs were 10 mm thick rectangular acrylic plates, with the same width as the flume. All of the experiments conducted as part of this study were of sufficient duration to ensure measured scour depths are in the equilibrium stage. The experimental conditions and the measured scour depths of all the tests are summarized in Table 2.

The capital letters of test codes used in Table 2 have the following meanings: C is for coarse sand, F is for fine sand, W represents weir height, D represents tailwater depth; the numbers following the letters (W and D) indicate the corresponding values of the weir height (z) and the tailwater depth (h_t) in millimetres.

2.1 *Coarse sand tests*

Guan et al. (2015) developed a data processing technique for scour measurement at submerged weirs in live-bed scour conditions. They studied three groups of coarse sand tests (CW30D150, CW40D150, and CW50D150). To further investigate the weir height effect and tailwater depth effect, two groups of coarse sand tests (CW20D150 and CW30D120) were conducted in this study.

The scour evolution at the weir and the bed elevation changes in the approach flow were measured using a Seatek multiple transducer array (MTA), which is an ultrasonic ranging system and can instantaneously measure the distance from the transducer surfaces to reflective objects under the water with an accuracy of $\pm$ 1 mm. The vertical velocity profiles in the approach flow were measured using a Nortek Vectrino + (Nortek, Rud, Norway) and integrated to determine the flow rates for each test. The tailwater levels were controlled by the level of the overflow pipe in the sump at the end of the flume. The average water level difference for each test was measured using a point gauge with a precision of $\pm$ 1 mm. All coarse sand tests were carried out in live-bed scour conditions. The layout of transducers, the measurement of bed elevations and flow conditions, and data processing procedures follow the description by Guan et al. (2015).

2.2 *Fine sand tests*

Three groups of fine sand tests (FW20D120, FW20D150, and FW30D150) were conducted in this study. During preliminary tests, it was found that the Seatek multiple transducers used in coarse sand tests are not suitable for the bed elevation measurement in fine sand tests under live-bed scour conditions. Near the bed, especially in the scour holes upstream and downstream of the weir, the concentration of suspensions under live-bed scour conditions is very high. The sand "cloud" formed above the bed significantly contaminates the signal transmission between the bed and the transducers. Thus, instead of ultrasonic transducers, webcams were employed for scour measurement in fine sand tests. As shown in Fig. 3, two Logitech HD webcams (Logitech, Lausanne, Switzerland), mounted on two rests, were placed symmetrically, with one on each side of the flume. Transparent grid sheets were placed on the glass walls for bed profile recording. The locations of webcams and the distance between webcams and flume glass walls were determined based on the webcam's diagonal field of view (78°) and scour-hole lengths. Image analysis was implemented to obtain bed profiles over time. The scour profiles were captured for each test from consecutive pictures taken at regular time intervals. The accuracy of scour depth measurement is $\pm$ 2 mm.

For non-ripple forming sand, clear-water scour conditions prevail up to the critical shear velocity value ($u_*/u_{*c} \approx 0.95$), while for ripple forming sand, the development of ripples could occur for $u_*/u_{*c} \geq 0.5$ (Ettema, 1980; Melville, 1984). To be consistent with the coarse sand tests, the channel bed upstream of the weir was made as a fixed bed for fine sand tests to prevent the development of ripples in clear-water scour conditions.

Table 1 Characteristics of sediment used in this study

Type	d_{16} (mm)	d_{30} (mm)	d_{50} (mm)	d_{84} (mm)	d_{90} (mm)	σ_g	Δ	u_{*c} (m s^{-1})
Fine sand	0.16	0.22	0.26	0.36	0.43	1.5	1.65	0.013
Coarse sand	0.65	0.73	0.85	1.10	1.15	1.3	1.65	0.027

Table 2 Summary of experimental conditions and results

TEST CODES	No.	t (h)	Q (m^3/s)	h_0 (mm)	H_d (mm)	h_a (mm)	U_0 (m/s)	U_c (m/s)	S_0	F	d_{s_a} (mm)	d_{s_max} (mm)	d_{us_a} (mm)	d_{us_max} (mm)
FW20D120	1	43.3	0.0150	121	1	0	0.281	0.263	0.0009	0.26	22	30	26	43
	2	22.2	0.0233	122	2	0	0.434	0.263	0.0016	0.40	41	45	43	83
	3	6.8	0.0305	121	2	1	0.574	0.263	0.0021	0.53	80	100	55	100
	4	4.7	0.0383	120	3	3	0.725	0.263	0.0026	0.67	88	112	54	100
	5	2.6	0.0467	120	2	2	0.884	0.263	0.0033	0.81	98	118	0	0
	6	3.3	0.0498	119	1	2	0.952	0.262	0.0040	0.88	129	145	0	0
FW20D150	7	37.7	0.0202	151	1	0	0.304	0.270	0.0009	0.25	17	18	33	48
	8	17.1	0.0330	151	2	1	0.496	0.270	0.0015	0.41	45	48	41	68
	9	6.6	0.0388	151	3	2	0.584	0.270	0.0020	0.48	50	62	55	90
	10	3.5	0.0486	151	4	3	0.732	0.270	0.0024	0.60	55	70	50	85
	11	2.2	0.0571	147	3	6	0.883	0.269	0.0033	0.74	75	95	0	0
	12	2.1	0.0640	148	3	5	0.983	0.270	0.0037	0.82	100	105	0	0
FW30D150	13	24.0	0.0101	150	0	0	0.153	0.270	0.0003	0.13	0	0	–[a]	–[a]
	14	216.0	0.0129	150	0	0	0.195	0.270	0.0005	0.16	31	31	–[a]	–[a]
	15	672.0	0.0176	151	1	0	0.265	0.270	0.0007	0.22	123	123	–[a]	–[a]
	16	52.2	0.0194	149	1	2	0.295	0.270	0.0009	0.24	38	45	29	48
	17	17.5	0.0290	149	3	4	0.442	0.270	0.0014	0.37	87	100	42	63
	18	7.5	0.0395	147	6	9	0.610	0.269	0.0020	0.51	97	120	57	110
	19	5.5	0.0485	141	9	18	0.782	0.268	0.0027	0.66	101	127	45	110
	20	3.0	0.0561	145	10	15	0.879	0.269	0.0033	0.74	116	127	0	0
	21	2.8	0.0630	148	10	12	0.968	0.270	0.0038	0.80	138	150	0	0
CW20D150	22	22.4	0.0337	150	6	6	0.511	0.367	0.0012	0.42	42	57	21	47
	23	20.7	0.0418	153	7	4	0.620	0.368	0.0017	0.51	46	92	81	136
	24	26.0	0.0503	157	10	3	0.728	0.369	0.0024	0.59	47	78	89	146
	25	9.0	0.0583	161	14	3	0.824	0.370	0.0033	0.66	52	83	93	131
	26	11.0	0.0640	164	17	3	0.887	0.371	0.0040	0.70	56	92	94	138
	27	3.2	0.0689	167	20	3	0.938	0.372	0.0046	0.73	68	105	92	149
	28	1.2	0.0790	170	24	4	1.056	0.373	0.0054	0.82	73	100	80	124
	29	1.1	0.0860	174	28	4	1.124	0.375	0.0057	0.86	75	100	78	127
CW30D120	30	96.0	0.0226	121	10	9	0.425	0.355	0.0012	0.39	73	106	7	19
	31	25.6	0.0251	127	13	6	0.449	0.358	0.0017	0.40	69	104	16	33
	32	25.5	0.0280	129	15	6	0.493	0.359	0.0021	0.44	63	96	47	87
	33	12.9	0.0307	130	17	7	0.537	0.359	0.0027	0.48	60	86	54	101
	34	12.5	0.0347	130	18	8	0.608	0.359	0.0032	0.54	64	92	60	110
	35	5.1	0.0452	132	23	11	0.779	0.360	0.0051	0.68	73	105	72	114
	36	3.1	0.0562	140	31	11	0.913	0.363	0.0065	0.78	112	140	85	160
	37	1.2	0.0655	143	36	13	1.041	0.364	0.0080	0.88	134	155	67	103

[a]No scour data was collected in clear-water scour conditions due to the fix bed upstream of the weir.

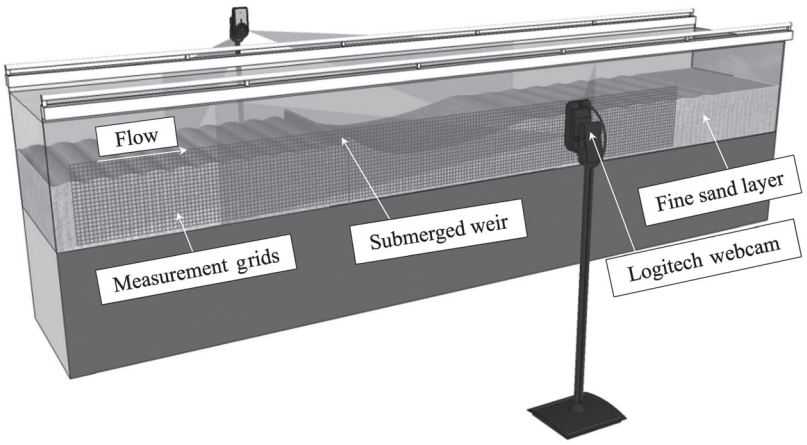

Figure 3 Experimental set-up for fine sand tests

Such a situation corresponds to field conditions where sediment supply is cut off upstream of the weir and also can be regarded as a scaled-down representation of large prototypes, which have no ripples forming upstream of the weir. The scour process upstream of the weir in clear-water scour conditions is not investigated in this study. For live-bed scour conditions, although the flow and weirs are two dimensional, the scour holes that formed upstream and downstream of the weir were three-dimensional because of the migrating three-dimensional ripples and the unsteady secondary flows developed within the scour holes around the weir. The observations show that the maximum scour depth occurs close to the flume side walls for most of the time during each live-bed scour test. Therefore, the maximum scour depths captured from the side walls are assumed to represent the scour depths that occurred within the scour areas around the weir. Scour depths upstream (d_{us}) and downstream (d_s) of the weir were recorded at regular time intervals throughout the duration of each experiment. The equilibrium scour depths (d_{us_a} and d_{s_a}) were taken as the time-averaged values of the scour depth recordings once equilibrium had been reached. Maximum observed scour depths ($d_{us\_\max}$ and $d_{s\_\max}$) were also recorded.

As for the experimental programme for the coarse sand tests reported in Guan et al. (2015), for all fine sand tests, the bed was initially flattened and a different flowrate, Q, was applied. The slope of the flume was adjusted to achieve the normal tailwater depth, h_t. In this study, two tailwater depths, h_t (120 and 150 mm), and two weir heights, z (20 and 30 mm), were used. The water level difference across the weir, H_d, and the average upstream aggradation height, h_a, were measured in the equilibrium stage using a point gage. The average approach flow depth, h_0, is calculated as $h_0 = h_t + H_d - h_a$. The critical average approach velocity, U_c, is determined from the logarithmic form of the velocity profile $U_c/u_{*c} = 5.75\ \log(5.53h_0/d_{50})$. The Froude number of the upstream flow, F, was in the range of 0.13 to 0.88.

3 Analysis and discussion

3.1 *Flow regimes over the weir*

Wu and Rajaratnam (1996) defined the boundary lines for SFR and IJR based on their experimental data. Their expressions for the boundary lines are as follows:

$$\text{SFR boundary: } (h_t - z)/(h_0 - z) = 1 - 0.215X + 0.0142X^2 - 0.00031X^3 \quad (1a)$$

$$\text{IJR boundary: } (h_t - z)/(h_0 - z) = 1 - 0.126X + 0.0076X^2 - 0.00017X^3 \quad (1b)$$

in which the dimensionless parameter $X = \sqrt{gH_d}/(q/h_t)$, and q is flowrate per unit width. The two boundary equations

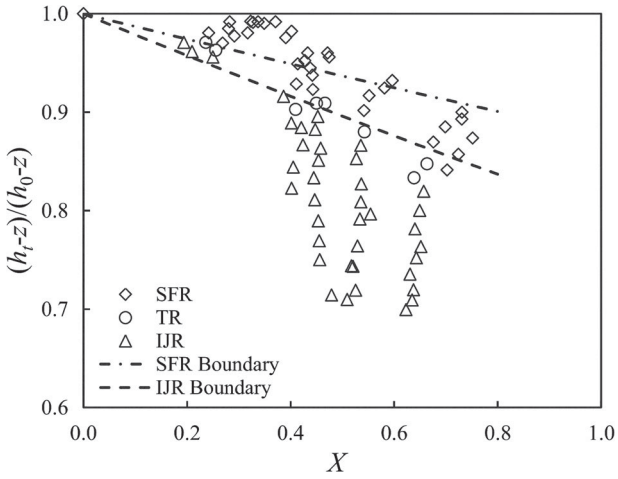

Figure 4 Comparison of experimental data with Eq. (1)

and the experimental data points from this study are plotted together in Fig. 4. As described in Wu and Rajaratnam (1996), the SFR zone is above the SFR boundary curve; the IJR zone is below the IJR boundary curve. Between these two boundary curves is the TR zone, in which the flow regime can switch from one to the other by an external disturbance. These two boundaries were derived under the experimental ranges of $1.43 \le X \le 20.98$ and $0 \le \mathsf{F} \le 0.23$. The results ($0 \le X \le 0.73$ and $0 \le \mathsf{F} \le 0.88$) presented in this research are outside these ranges, and only roughly match these two boundaries (Fig. 4).

As demonstrated in previous literature (Guan et al., 2015; Wu & Rajaratnam, 1996, 1998), the flow regime over the weir is dependent on the water level difference across the weir. For submerged flow conditions, the water level difference across the weir is dependent on the flow rate, weir height and tailwater depth. Therefore, flow regimes over the submerged weir could be represented as a function of upstream Froude number, F, and dimensionless parameter z/h_t. As seen in Fig. 5, the trends of the data from Guan et al. (2015) and from this study are consistent with the results from Wu and Rajaratnam (1996) and extend the experimental ranges for the flow regime research. Using the TR experimental data from literature and this study, the TR boundary line could be approximately expressed as:

$$\mathsf{F} = -0.35\ \ln\left(\frac{z}{h_t}\right) + 0.01 \quad (2)$$

Equation (2) has a coefficient of determination $R^2 = 0.97$ and is valid for $0 < \mathsf{F} < 0.72$, $0.13 < z/h_t < 1$. In Fig. 5, the IJR zone is above the TR boundary line and the SFJ zone is below the TR boundary line.

Using the data for all flow regimes in Guan et al. (2015) and this study, the data points (F, z/h_t) are plotted in Fig. 6. The results indicate that TR occurs at the value of the dimensionless parameter $\mathsf{F}(z/h_t)^{0.4} \approx 0.3$, which deviates slightly from Eq. (2). The deviation is caused by different experimental conditions of the regression data. The data from Wu and Rajaratnam (1996)

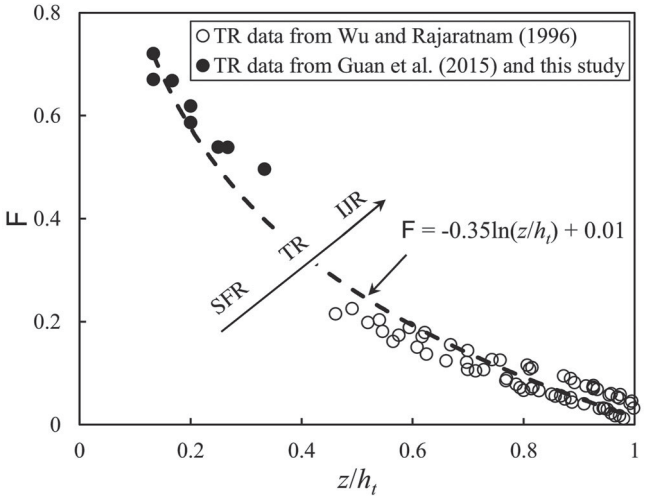

Figure 5 TR data from the literature and this study

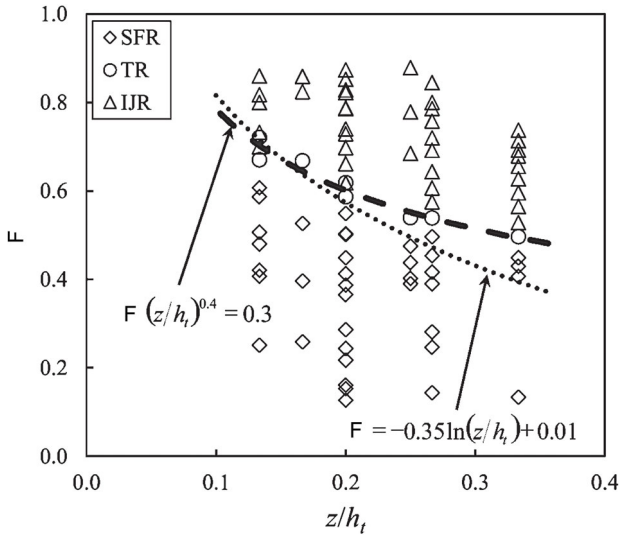

Figure 6 Comparison of two TR boundary equations, using the experimental data from this study and Guan et al. (2015)

were collected in fixed bed experiments, while the experiments in Guan et al. (2015) and this study were undertaken with a movable bed, which has migrating bedforms and scour holes at the weir. For a movable bed with scouring at the weir, the bed roughness and form drag increase the approach flow depth, and the scour hole downstream of the weir provides a larger energy dissipating zone in the tailwater than that formed in the fixed bed conditions.

3.2 *Sediment size effect*

To study the sediment size effect on scouring at submerged weirs, the data in this study and Guan et al. (2015) are compared in Fig. 7. For live-bed scour conditions, the observations show that the scour depth upstream of the rectangular submerged weir in fine sand tests follows a scour-and-fill process due to the periodic approaching ripples, which is consistent with the coarse sediment tests. The normalized scour depth upstream of the weir for fine sediment tests has the same trend as that for coarse sediment tests (it initially increases and then decreases as the flow intensity increases), but with a smaller magnitude (Fig. 7a). This is because the ripples formed in the fine sediment tests are smaller than the bedforms in the coarse sediment tests.

In clear-water scour conditions for both sediment sizes, the normalized scour depth downstream of the weir increases as the flow intensity increases (Fig. 7b). The decrease of sediment size reduces the scour depth downstream of the weir. In live-bed scour conditions, the trends of normalized scour depths for two sediment sizes both first decrease then increase again as flow intensity increases. However, for fine sand tests, the minimum equilibrium scour depth downstream of the weir occurs immediately after the transition from clear-water scour conditions to live-bed scour conditions ($U_0/U_c = 1$), where the flow regime over the weir is still in the SFR condition. For the coarse sand tests the equilibrium scour depth keeps decreasing after $U_0/U_c = 1$ until the flow regime over the weir becomes the TR condition, where the minimum is reached (Fig. 7b). In SFR conditions, the scour hole downstream of the weir is induced by the increasing jet thickness and turbulence mixing with the tailwater. The turbulence intensity within the recirculation zone downstream of the weir governs the dimensions of the scour hole (Guan et al., 2014). Because the sediment settling velocities (w) of the fine and coarse sands are different ($w_1 = 1.3$ cm s^{-1} for $d_{50} = 0.26$ mm and $w_2 = 10.9$ cm s^{-1} for $d_{50} = 0.85$ mm; Cheng, 1997), the live-bed scour processes downstream of the weir under SFR conditions present different characteristics. For the coarse sediment under SFR conditions, the increasing flow intensities near the downstream scour bed are not large enough to lift and remove all the upstream sediment input as flow intensity increases; this causes a decreasing trend of the downstream scour depth after $U_0/U_c = 1$. For fine sediment, the sediment settling velocity is much smaller than for coarse sediment, the flow in the scour hole can transport all the incoming sediment and the sediment from the downstream scour hole under SFR conditions as flow intensity increases; this causes an increasing trend of the downstream scour depth after $U_0/U_c = 1$. For IJR, the scour depth for both sediment sizes increases with increasing flow intensity.

In fine sand tests, the normalized scour depth upstream of the weir reaches zero when the flow intensity reaches 3.25 (Fig. 7), at which the upstream bed enters the plane bed condition (upper regime). However, the scour depth downstream of the weir continues to increase thereafter. This is different from live-bed scour at bridge piers and abutments. It can be inferred that in the upper regime of bedforms, although the upstream sediment supply is increasing, the scour depth downstream of the weir remains controlled mainly by the increasing forces of the impinging jet over the weir. The balance of the increasing scour rate downstream of the weir and the increasing upstream sediment supply rate is expected to occur at a flow intensity greater than 3.8, which is the upper limit of the experimental range in this study.

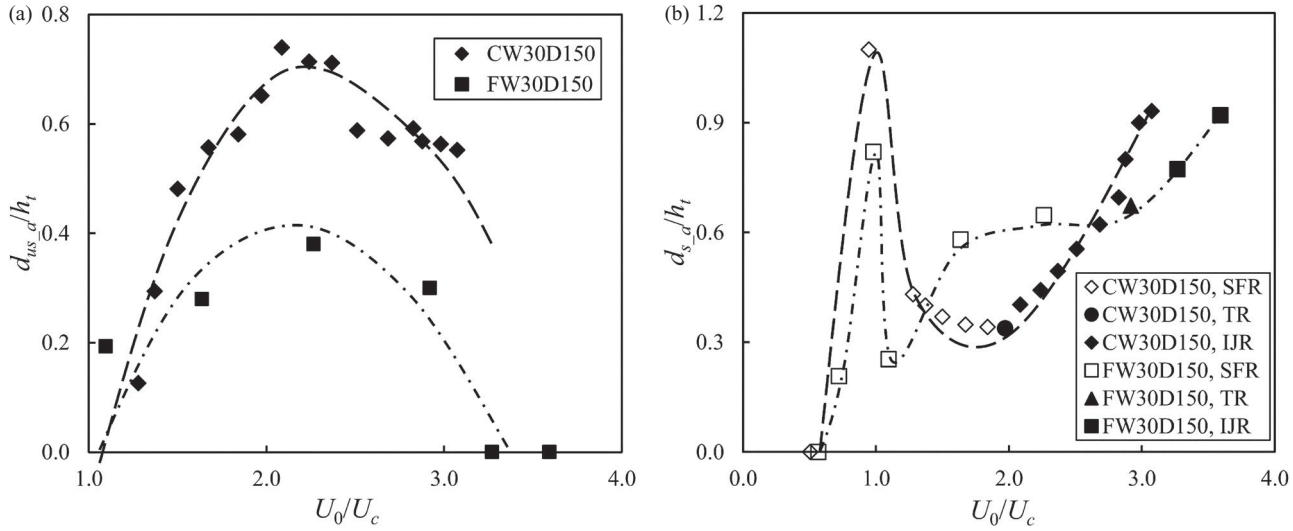

Figure 7 Sediment size effect on scouring at submerged weirs: (a) upstream normalized equilibrium scour depth versus flow intensity; (b) downstream normalized equilibrium scour depth versus flow intensity

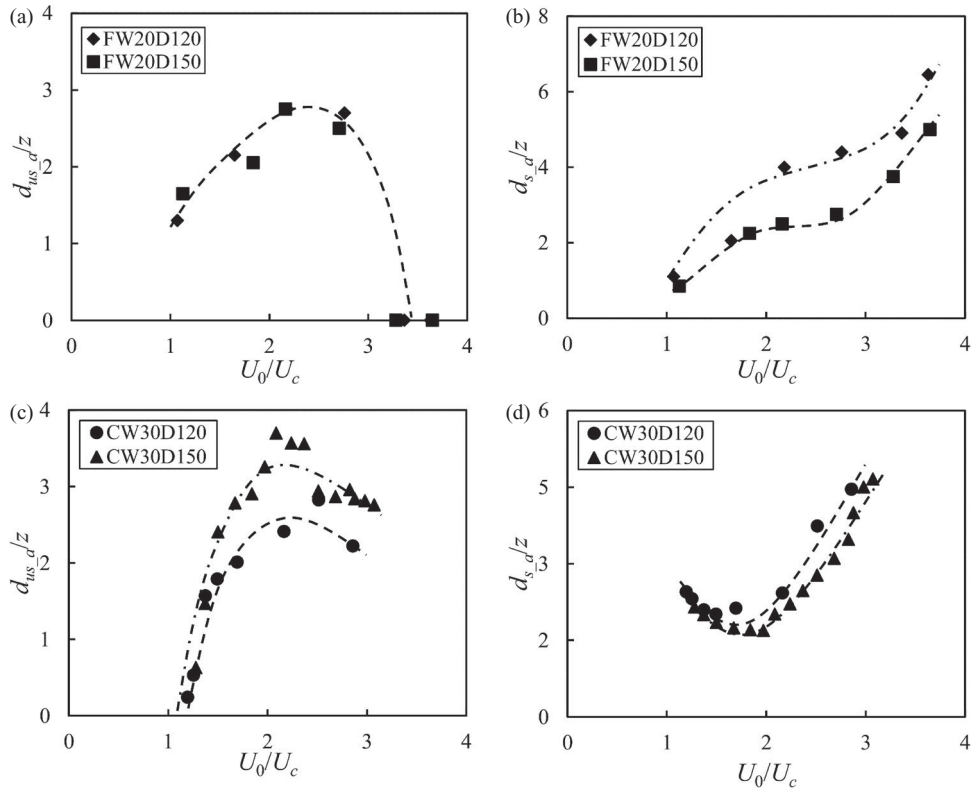

Figure 8 Tailwater depth effect on scouring at submerged weirs: (a) upstream normalized equilibrium scour depth versus flow intensity, fine sand tests; (b) downstream normalized equilibrium scour depth versus flow intensity, fine sand tests; (c) upstream normalized equilibrium scour depth versus flow intensity, coarse sand tests; (d) downstream normalized equilibrium scour depth versus flow intensity, coarse sand tests

3.3 *Tailwater depth effect under live-bed conditions*

The results from this study and Guan et al. (2015) are plotted in Fig. 8. Two tailwater depths (120 mm and 150 mm) were used in both coarse and fine sand tests.

For scouring upstream of the weir, the decrease of the tailwater depth has an insignificant effect on the magnitude of the scour depth in fine sand tests, while in coarse sand tests it decreases the scour depth (Fig. 8a and c). As reported by Guan et al. (2015), the magnitude of scour depth is dependent on the weir height and the size of the approaching bedforms. For dune-forming sand, the bedform height and length are dependent on flow depth and sediment size; while for ripple-forming sand, the size properties of the ripples are more dependent on the sediment size and less sensitive to the flow depth. In this study, with a fixed weir height, the approach flow depth decreases when the tailwater depth decreases. It was observed that the average ripple

sizes are similar in tests FW20D120 and FW20D150, while the average dune size in test CW30D150 is larger than that in test CW30D120. This explains the effect of tailwater depth on the scour depth upstream of the weir in Fig. 8a and c.

For scouring downstream of the weir, the decrease of tailwater depth increases the scour depth downstream of the weir in both fine and coarse sand tests (Fig. 8b and d). This is because the decrease of the tailwater depth increases the jet power over the weir, which has a direct impact on the scour bed downstream of the weir.

3.4 *Dimensional analysis of local scour*

The geometry of the submerged weir under live-bed scour conditions is sketched in Fig. 1. The main parameters that determine the scour depth around the weir are:

$$y = f\,(\rho, \nu, g, h_0, h_t, U_0, \rho_s, d_{50}, \sigma_g, U_c, b, z) \tag{3}$$

where y is scour depth parameter (d_{us_a},d_{s_a}); ν is fluid kinematic viscosity; g is acceleration of gravity; ρ,ρ_s are densities of water and sediment, respectively; and b is weir width. Eq. (3) includes a consideration of approach flow and tailwater conditions (ρ, ν, g, h_0, h_t, U_0), sediment characteristics and transport (ρ_s, d_{50}, σ_g, U_c), and structure geometry (b, z).

In this study, weir width was kept constant. The approach flow depth is dependent on the flow intensity and weir height. Uniform sediments were used. Thus, assuming constant relative density of sediment and fluid viscosity, a dimensionless expression for the equilibrium scour depth at submerged weirs can be developed from Eq. (3):

$$\frac{y}{h_t} = f\left(\frac{U_0}{U_c}, \frac{z}{h_t}, \frac{d_{50}}{h_t}\right) \tag{4}$$

In this study, the flow intensity and normalized weir height ranges are $0 \le U_0/U_c \le 3.65$, $0.13 \le z/h_t \le 0.33$ and $0.0017 \le d_{50}/h_t \le 0.0071$ respectively.

3.5 *Equilibrium scour depth downstream of the weir*

On the basis of the analysis in the previous sections, the scour depth downstream of the weir is directly dependent on weir height and inversely dependent on tailwater depth for all the tests. Since only two uniform sands are used, a monotonic relationship between d_{50} and d_{s_a} is assumed in this study. Therefore, Eq. (4) can be assumed to have the following structure:

$$\frac{d_{s\_a}}{h_t} = i\left(\frac{z}{h_t}\right)^j \left(\frac{d_{50}}{h_t}\right)^k f\left(\frac{U_0}{U_c}\right) \tag{5}$$

in which i, j, and k are coefficients. To determine the function of flow intensity, the scour conditions need to be considered separately. For clear-water scour conditions, the scour depth

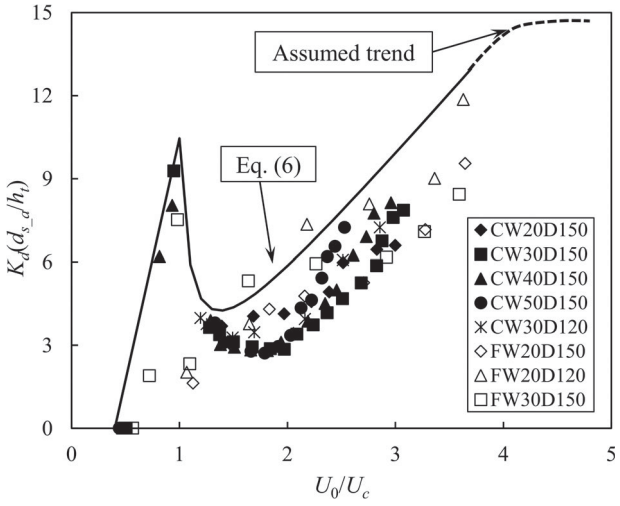

Figure 9 Equilibrium scour depth downstream of the weir

downstream of the weir increases with increasing flow intensity. For live-bed scour conditions, flow intensity effects on the scour depth downstream of the weir become complicated, accounting for different types of bedforms and flow regimes over the weir. It is very difficult to propose a single relationship between the scour depth downstream of the weir and flow intensity for both fine and coarse sand tests in live-bed scour conditions (see Fig. 7b). Therefore, an envelope function with a discontinuity at $U_0/U_c = 1$ enclosing almost all experimental data for scour downstream of the weir is adopted in this study. On the basis of the experimental data, the envelope equation (Eq. 6) is derived as:

$$\frac{d_{s\_a}}{h_t} = 17.42\left(\frac{z}{h_t}\right)^{1.10}\left(\frac{d_{50}}{h_t}\right)^{0.07}\left(\frac{U_0}{U_c} - 0.4\right) \quad 0.4 < U_0/U_c \le 1 \tag{6a}$$

$$\frac{d_{s\_a}}{h_t} = 4.50\left(\frac{z}{h_t}\right)^{1.10}\left(\frac{d_{50}}{h_t}\right)^{0.07}\left[\left(\frac{U_0}{U_c} - 0.90\right) + \frac{0.23}{\left(\frac{U_0}{U_c} - 0.90\right)}\right] \quad 1 < U_0/U_c \le 3.65 \tag{6b}$$

Using coefficient $K_d = (z/h_t)^{-1.10}(d_{50}/h_t)^{-0.07}$, Eq. (6) and the experimental data are plotted in Fig. 9. Because the scour depth downstream of the weir cannot increase indefinitely in live-bed scour conditions, an upper limit for scour depth is expected for flow intensity greater than 3.65 (see the assumed trend in Fig. 9).

3.6 *Comparison of existing equations for equilibrium scour depth downstream of the weir*

The relevant existing equations for equilibrium scour depth downstream of rectangular weirs are listed in Table 3. Refer to Fig. 1 for the common parameters used in these equations.

Table 3 Existing prediction equations for equilibrium scour depth downstream of a rectangular weir

Authors	Equations
Bormann and Julien (1991)	$d_{s\_a} = \frac{Kq^{0.6}U_w \sin\beta}{g^{0.8}d_{90}^{0.4}} - z$ $\beta = 0.316\sin\lambda + 0.15\ln\left(\frac{h_0}{h_0 - z}\right) + 0.13\ln\left(\frac{h_t}{h_0 - z}\right) - 0.05\ln\left(\frac{U_w}{\sqrt{g(h_0 - z)}}\right)$ $K = C_d^2\{\rho\sin\varphi/[\sin(\varphi + \beta)C_f(\rho_s - \rho)]\}^{0.8}$ where U_w = average velocity on the weir; λ = face angle of the weir; C_d = jet diffusion coefficient (taken as 1.8); φ = sediment repose angle (taken as 36°); β = downstream face slope angle; and C_f = local friction coefficient (taken as 2.0)
D'Agostino and Ferro (2004)	$\frac{d_{s\_a}}{z} = 0.540\left(\frac{b}{z}\right)^{0.593}\left(\frac{h_t}{H_d}\right)^{-0.126}\left(\frac{Q}{bz\sqrt{gd_{50}\Delta}}\right)^{0.544}\left(\frac{d_{90}}{d_{50}}\right)^{-0.856}\left(\frac{b}{B}\right)^{-0.751}$ where B = channel width; b = weir width; Q = flowrate
Marion et al. (2006)	$\frac{d_{s\_a}}{H_s} = 3.0\left(\frac{a_1}{H_s}\right)^{0.60} SI^{-0.19}\left(1 - e^{-0.25\frac{L}{H_s}}\right)$ where H_s = critical specific energy; SI = sediment sorting index, calculated as $0.5(d_{84}/d_{50} + d_{50}/d_{16})$; L = distance between weirs; a_1 = morphological jump
Ben Meftah and Mossa (2006)	$\frac{d_{s\_a}}{H_s} = 0.59\frac{\Delta LS_0}{H_s} + 1.74$ where S_0 = initial sand bed slope
Pagliara and Kurdistani (2013)	$\frac{d_{s\_a}}{z} = 1.3\left[\frac{b}{B}(1 + S_0^{0.1})\right]^{0.9}\left(\frac{\mathsf{F}_d^2 H_d}{z}\right)^{0.4}$ $\mathsf{F_d} = Q/\left(bz\sqrt{gd_{50}\Delta}\right)$ where $\mathsf{F_d}$ = densimetric particle Froude number

Figure 10 and Table 4 show the results of applying the relevant existing equations in Table 3 to the data produced in this study. Because there is only one weir in this study, the distance between two sequent weirs is assumed to be infinite. The morphological jump "a_1" in Marion et al. (2006) and the product "LS_0" in Ben Meftah and Mossa (2006) are taken as the weir height z in this study. The initial sand bed slope in Pagliara and Kurdistani (2013) is taken as the flume bed slope, S_0, in Table 2. The values shown in Table 4 are the percentage of underpredictions and the percentage of overpredictions over 300%. The equations used in Fig. 10b, c, e and f do not consider the effects of the upstream sediment supply and are designed for the impinging jet flow over an unsubmerged weir. Therefore, most of the predictions from these existing equations are greatly overestimated. For the equation plotted in Fig. 9d, the performance is relatively better than for other existing equations on account of a consideration of the upstream sediment supply. Interestingly, the data points in Fig. 9b–f show a similar pattern. This is because all existing equations are designed for unsubmerged or partially submerged weirs, which do not have the change of flow regimes over the weir. The relationship between their predicted scour depths and flow intensity was assumed to be a monotonic function.

3.7 *Equilibrium scour depth upstream of the weir*

The form of Eq. (5) is also adopted for the prediction of the equilibrium scour depth upstream of the weir. A parabolic relationship is assumed for the function of the flow intensity. Using the experimental data, the normalized equilibrium scour depth upstream of the weir can be expressed as:

$$\frac{d_{us\_a}}{h_t} = 3.40\left(\frac{z}{h_t}\right)^{-0.13}\left(\frac{d_{50}}{h_t}\right)^{0.52}\left(\frac{U_0}{U_c} - 0.65\right)\left(3.90 - \frac{U_0}{U_c}\right) \quad 1 < U_0/U_c \le 3.65 \tag{7}$$

Using coefficient $K_u = (z/h_t)^{0.13}(d_{50}/h_t)^{-0.52}$, Eq. (7) and the experimental data are plotted in Fig. 11. The scour depth upstream of the weir is assumed to decrease to zero in the range that flow intensity is greater than 3.65 (see the assumed trend is Fig. 11).

3.8 *Design of the maximum scour depth*

For the design estimation of live-bed scour at a hydraulic structure, the bedform effect (bedform height, η) should be added to the equilibrium scour depths at the structure to obtain the total scour depth (Chiew & Melville, 1987;

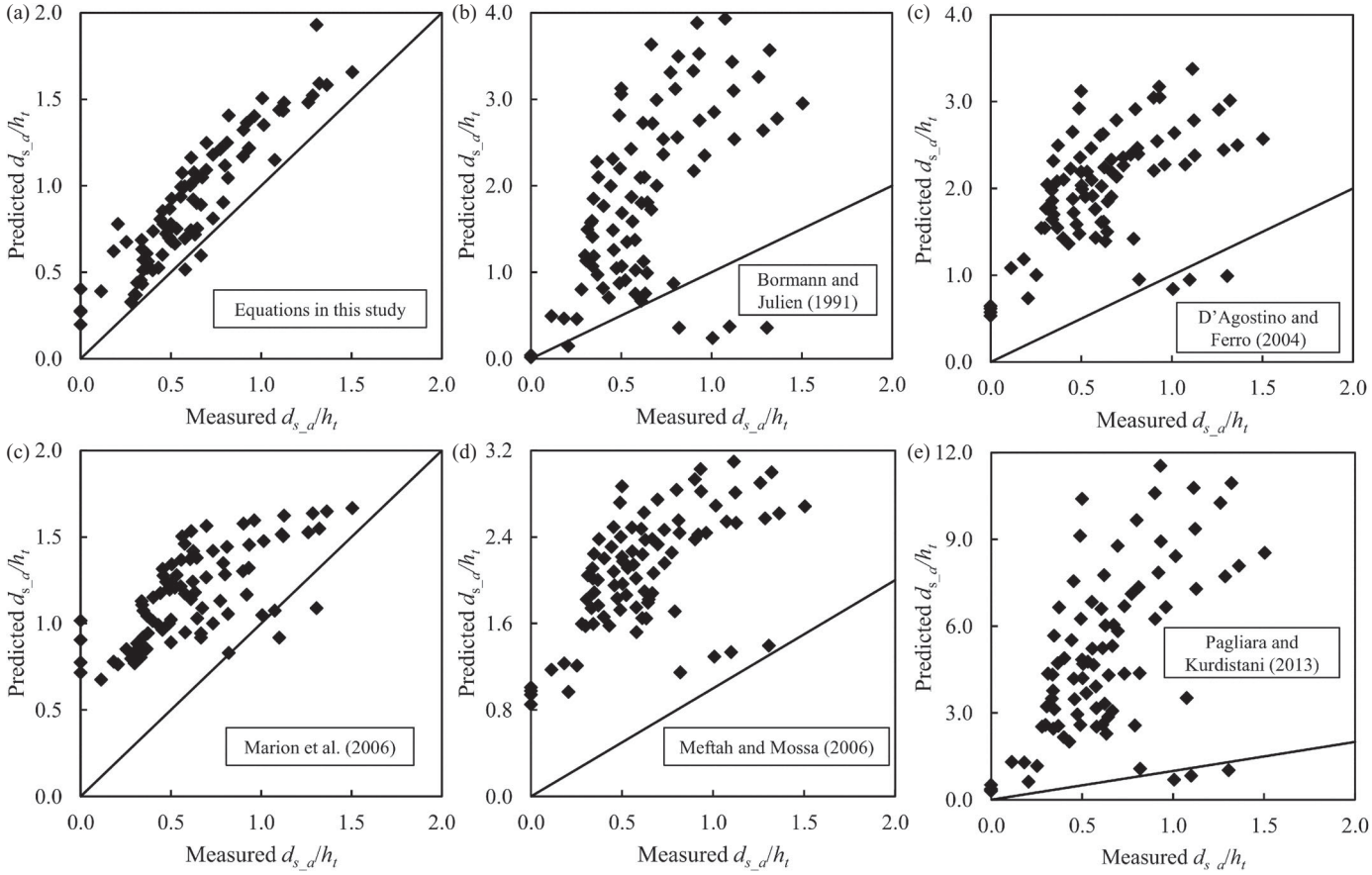

Figure 10 Comparison of measured equilibrium scour depths with predicted equilibrium scour depths using existing equations. Solid line on all plots denotes "perfect fit"

Table 4 Comparisons of measured equilibrium scour depths with predicted equilibrium scour depths using existing equations

Equations	Underpredictions	Overpredictions > 300%
This study	2.4%	8.2%
Bormann and Julien (1991)	5.9%	49.4%
D'Agostino and Ferro (2004)	3.5%	70.6%
Marion et al. (2006)	3.5%	12.9%
Ben Meftah and Mossa (2006)	0%	68.2%
Pagliara and Kurdistani (2013)	3.5%	95.3%

Sheppard & Miller, 2006). For scour at submerged weirs, Guan et al. (2015) developed a measurement and data process technique for extracting bedform properties (length, height and celerity) and proposed the following equations:

$$d_{us\_\max} \approx (d_{us\_a} + 1.3\eta_m) \tag{8a}$$

$$d_{s\_\max} \approx (d_{s\_a} + \eta_m) \tag{8b}$$

in which η_m is measured bedform height. However, instead of measured data, the bedform amplitudes should be estimated at the design stage of local scour. In this study, the upstream bedform height is not measured and a practical prediction is obtained from Eq. (9) for bedform height calculation (van Rijn, 1984):

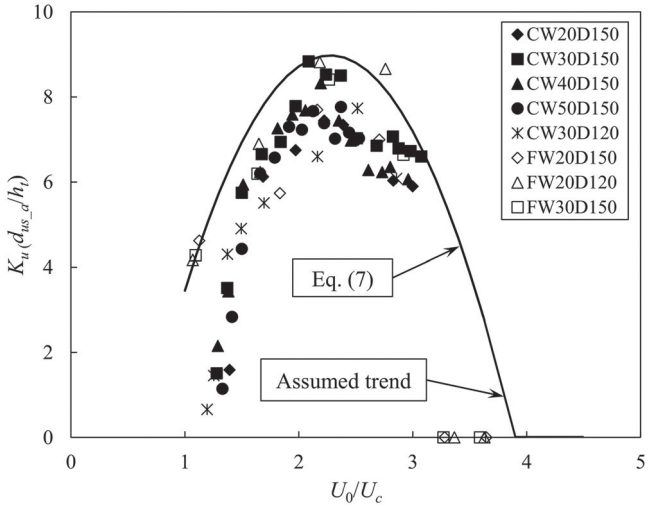

Figure 11 Equilibrium scour depth upstream of the weir. Solid line on all plots denotes 'perfect fit'

$$\frac{\eta_c}{h_0} = 0.11\left(\frac{d_{50}}{h_0}\right)^{0.3}(1 - e^{-0.5T})(25 - T) \tag{9}$$

$$T = \frac{{u'_*}^2 - u_{*c}^2}{u_{*c}^2} \tag{10}$$

in which u'_* is the shear velocity related to grains and is obtained using the method of Yang, Tan, and Lim (2005). The calculated

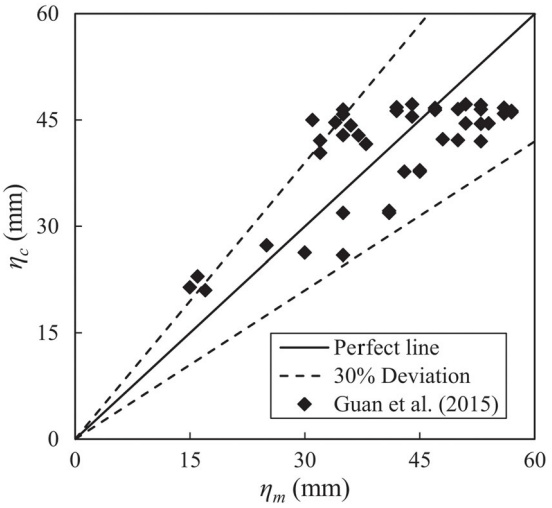

Figure 12 Comparison between measured bedform height and calculated bedform height

bedform height, η_c, and the measured bedform height, η_m, from tests CW30D150, CW40D150 and CW50D150 (Guan et al., 2015), are compared in Fig. 12.

As seen in Fig. 12, over 90% of the data points are within the ±30% deviation lines, which implies that the chosen Eq. (9) predicts well the bedform height in the previous study. Therefore, the calculated bedform heights, η_c, can be obtained for all the tests by applying Eq. (9). The values of [d_{us_max}, (d_{us_a} + 1.3 η_c)] and [d_{s_max}, (d_{s_a} + η_c)] for all the tests are plotted in Fig. 13. Most of the data are located within the ±25% deviation from the perfect line (Fig. 13), except a few data points, for which the ripple heights are overestimated using Eq. (9). The results show that Eq. (8), proposed in Guan et al. (2015), is still valid.

For use of the prediction equations of equilibrium scour depth (Eqs (6) and (7)) in design, a conservative method for estimation of the maximum scour depth is proposed as

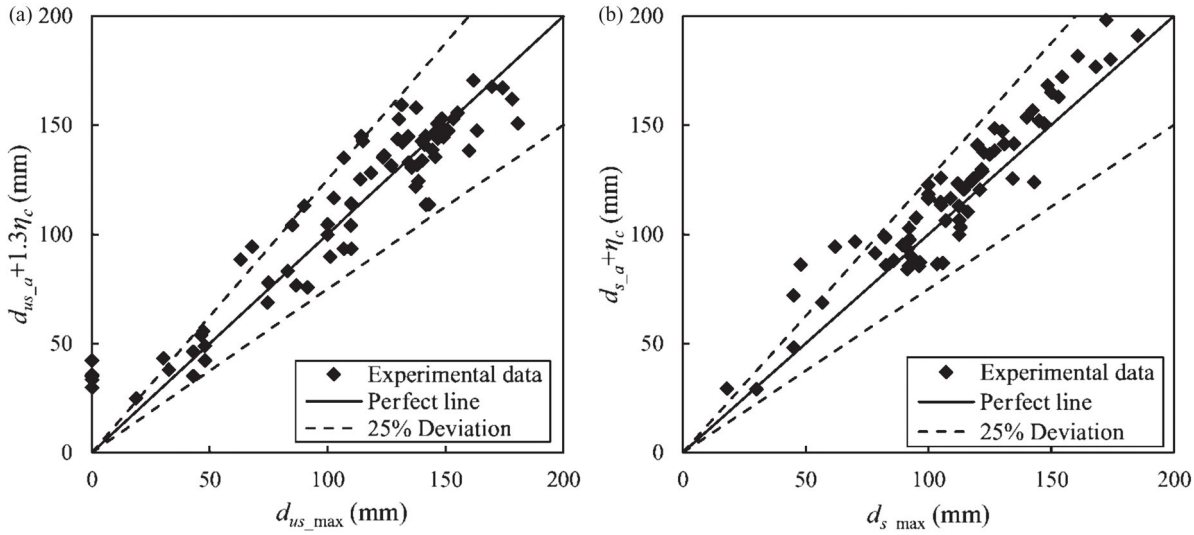

Figure 13 Comparison between measured maximum scour depth and adjusted equilibrium scour depth using Eq. (8): (a) upstream scour data; (b) downstream scour data

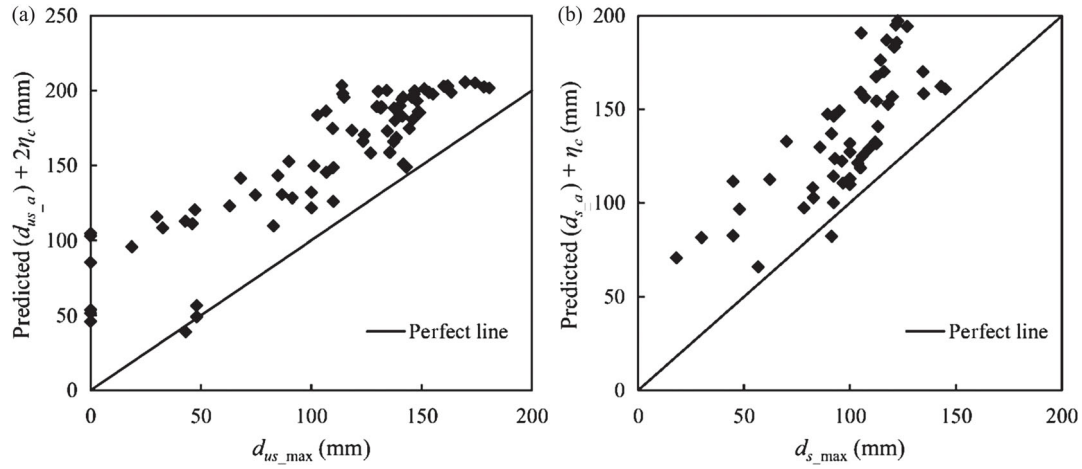

Figure 14 Comparison between measured maximum scour depth and adjusted predicted equilibrium scour depth by Eq. (11): (a) upstream scour data; (b) downstream scour data

follows:

$$d_{us\_\max} \approx \text{predicted}(d_{us\_a}) + 2\eta_c \quad (11a)$$

$$d_{s\_\max} \approx \text{predicted}(d_{s\_a}) + \eta_c \quad (11b)$$

All values of $[d_{s\_\max}, \text{predicted}(d_{us\_a}) + 2\eta_c]$, $[d_{s\_\max}, \text{predicted}(d_{s\_a}) + \eta_c]$ are plotted in Fig. 14.

4 Conclusions

This paper reports an experimental study of scour at submerged weirs in sand-bed channels. New scour data in both ripple-forming and dune-forming sand channels have been presented.

In clear-water scour conditions, the equilibrium scour depth downstream of the weir increases with increasing flow intensity, for both sediment sizes. The decrease of sediment size reduces the scour depth downstream of the weir.

In live-bed scour conditions, the equilibrium downstream scour depth first decreases then increases again as the flow intensity increases for both sediment sizes. However, the minimum equilibrium scour depth occurs at different flow intensities for the two different sediment sizes due to the effect of sediment size (different settling velocities) and flow regimes over the weir.

The normalized scour depth upstream of the weir for fine sediment tests experiences the same trend as coarse sediment tests (first increases then decreases) but with a smaller magnitude. The decrease of tailwater depth increases the scour depth downstream of the weir in both fine and coarse sand tests. Upstream of the weir, the scour depth is found to be sensitive to the size of bedforms.

A new TR boundary equation, expressed as a function of upstream Froude number and the ratio of weir height to tailwater depth, for all experimental data from the literature and this study is proposed. Updated prediction equations for equilibrium scour depth at submerged weirs are given, based on experimental data produced in Guan et al. (2015) and this study. The updated equations include the effects of flow intensity, sediment size, weir height, and tailwater depth. A design method for the maximum scour depths both upstream and downstream of the submerged weir is also developed.

Acknowledgements

The authors would like to acknowledge Dr Wu Shouhong and Professor N. Rajaratnam for their kind help in providing original experimental data from their published paper. The valuable suggestions from Dr Keith Adams are appreciated.

Funding

This work was supported by the Fundamental Research Funds for the Central Universities [No. 2013/B15020289]. The first author would like to thank the China Scholarship Council for financial support of this research.

Notation

The following symbols are used in this paper:

a_1 = morphology jump (m)
B = channel width (m)
b = weir width (m)
C_d = jet diffusion coefficient (–)
C_f = local friction coefficient (–)
d_{s_a} = equilibrium scour depth downstream of the weir (m)
$d_{s\_\max}$ = maximum scour depth downstream of the weir (m)
d_{us} = scour depth upstream of the weir in each measurement (m)
d_{us_a} = equilibrium scour depth upstream of the weir (m)
$d_{us\_\max}$ = maximum scour depth upstream of the weir (m)
d_s = scour depth downstream of the weir in each measurement (m)
d_x = sediment size, for which x% (in weight) of sediment particles are finer (m)
F = Froude number upstream of the weir (–)
$\mathsf{F_d}$ = densimetric particle Froude number (–)
g = acceleration of gravity (ms^{-2})
H_d = water level difference across the weir (m)
H_s = critical specific energy (m)
h_0 = average approach flow depth (m)
h_a = aggradation height (m)
h_t = tailwater depth (m)
i, j, k = coefficients that are determined from the experimental results (–)
L = distance between sequent weirs (m)
Q = flowrate ($\text{m}^3\ \text{s}^{-1}$)
q = flowrate per unit width ($\text{m}^2\ \text{s}^{-1}$)
R^2 = coefficient of determination (–)
S_0 = initial bed slope (flume bed slope) (–)
SI = sediment sorting index (–)
t = scour time (s)
U_0 = average approach flow velocity (m s^{-1})
U_c = critical average approach flow velocity (m s^{-1})
U_w = average velocity on the weir (m s^{-1})
u_* = shear velocity (m s^{-1})
u_{*c} = critical shear velocity (m s^{-1})
u'_* = shear velocity related to grains (m s^{-1})
X = dimensionless parameter for calculating TR boundaries (–)
y = scour depth parameter (d_{us_a}, d_{s_a}) (m)
z = weir height (m)
α = parameter for determining flow regime (–)
β = downstream face slope angle (°)
Δ = relative submerged particle density (–)
η_c = calculated bedform heights (m)
η_m = measured bedform heights (m)
λ = face angle of the weir (°)
ν = kinematic viscosity of fluid ($\text{m}^2\ \text{s}^{-1}$)
ρ = water density (kg m^{-3})
ρ_s = sediment density (kg m^{-3})

σ_g = standard deviation of sediment size (–)
φ = sediment repose angle (°)

References

Adduce, C., & La Rocca, M. (2006). Local scouring due to turbulent water jets downstream of a trapezoidal drop: Laboratory experiments and stability analysis. *Water Resources Research*, *42*(2), W02405. doi:10.1029/2005wr004139

Adduce, C., & Sciortino, G. (2006). Scour due to a horizontal turbulent jet: Numerical and experimental investigation. *Journal of Hydraulic Research*, *44*(5), 663–673.

Azimi, A., Rajaratnam, N., & Zhu, D. (2014). Submerged flows over rectangular weirs of finite crest length. *Journal of Irrigation and Drainage Engineering*, *140*(5), 06014001. doi:10.1061/(ASCE)IR.1943-4774.0000728

Ben Meftah, M., & Mossa, M. (2006). Scour holes downstream of bed sills in low-gradient channels. *Journal of Hydraulic Research*, *44*(4), 497–509.

Bhuiyan, F., Hey, R. D., & Wormleaton, P. R. (2009). Effects of vanes and W-weir on sediment transport in meandering channels. *Journal of Hydraulic Engineering*, *135*(5), 339–349.

Bormann, N. E., & Julien, P. Y. (1991). Scour downstream of grade-control structures. *Journal of Hydraulic Engineering*, *117*(5), 579–594.

Chen, Z., Shao, X., & Zhang, J. (2005). Experimental study on the upstream water level rise and downstream scour length of a submerged dam. *Journal of Hydraulic Research*, *43*(6), 703–709.

Cheng, N. S. (1997). Simplified settling velocity formula for sediment particle. *Journal of Hydraulic Engineering*, *123*(2), 149–152.

Chiew, Y. M., & Melville, B. W. (1987). Local scour around bridge piers. *Journal of Hydraulic Research*, *25*(1), 15–26.

Comiti, F., Cadol, D., & Wohl, E. (2009). Flow regimes, bed morphology, and flow resistance in self-formed step pool channels. *Water Resources Research*, *45*(4), W04424. doi:10.1029/2008wr007259

Comiti, F., & Lenzi, M. A. (2006). Dimensions of standing waves at steps in mountain rivers. *Water Resources Research*, *42*(3), W03411. doi:10.1029/2004wr003898

D'Agostino, V., & Ferro, V. (2004). Scour on alluvial bed downstream of grade-control structures. *Journal of Hydraulic Engineering*, *130*(1), 24–37.

Ettema, R. (1980). *Scour at bridge piers* (PhD Thesis). The University of Auckland, Auckland.

Fritz, H., & Hager, W. (1998). Hydraulics of embankment weirs. *Journal of Hydraulic Engineering*, *124*(9), 963–971.

Gaudio, R., Marion, A., & Bovolin, V. (2000). Morphological effects of bed sills in degrading rivers. *Journal of Hydraulic Research*, *38*(2), 89–96.

Guan, D., Melville, B. W., & Friedrich, H. (2014). Flow patterns and turbulence structures in a scour hole downstream of a submerged weir. *Journal of Hydraulic Engineering*, *140*(1), 68–76.

Guan, D., Melville, B. W., & Friedrich, H. (2015). Live-bed scour at submerged weirs. *Journal of Hydraulic Engineering*, *141*(2), 04014071. doi:10.1061/(ASCE)HY.1943-7900.0000954

Kabiri-Samani, A., Ansari, A., & Borghei, S. M. (2010). Hydraulic behaviour of flow over an oblique weir. *Journal of Hydraulic Research*, *48*(5), 669–673.

Lenzi, M. A., Marion, A., & Comiti, F. (2003a). Interference processes on scouring at bed sills. *Earth Surface Processes & Landforms*, *28*(1), 99–110.

Lenzi, M. A., Marion, A., & Comiti, F. (2003b). Local scouring at grade-control structures in alluvial mountain rivers. *Water Resources Research*, *39*(7), 1176.

Lenzi, M. A., Marion, A., Comiti, F., & Gaudio, R. (2002). Local scouring in low and high gradient streams at bed sills. *Journal of Hydraulic Research*, *40*(6), 731–739.

Lu, J. Y., Hong, J. H., Chang, K. P., & Lu, T. F. (2012). Evolution of scouring process downstream of grade-control structures under steady and unsteady flows. *Hydrological Processes*, *27*(19), 2699–2709.

Marion, A., Lenzi, M. A., & Comiti, F. (2004). Effect of sill spacing and sediment size grading on scouring at grade-control structures. *Earth Surface Processes and Landforms*, *29*(8), 983–993.

Marion, A., Tregnaghi, M., & Tait, S. (2006). Sediment supply and local scouring at bed sills in high-gradient streams. *Water Resources Research*, *42*(6), W06416. doi:10.1029/2005wr004124

Melville, B. W. (1984). Live-bed scour at bridge piers. *Journal of Hydraulic Engineering*, *110*(9), 1234–1247.

Melville, B. W. (1997). Pier and abutment scour: Integrated approach. *Journal of Hydraulic Engineering*, *123*(2), 125–136.

Pagliara, S., & Kurdistani, S. M. (2013). Scour downstream of cross-vane structures. *Journal of Hydro-environment Research*, *7*(4), 236–242.

van Rijn, L. (1984). Sediment transport, Part III: Bed forms and alluvial roughness. *Journal of Hydraulic Engineering*, *110*(12), 1733–1754.

Scurlock, S. M., Thornton, C. I., & Abt, S. R. (2012). Equilibrium scour downstream of three-dimensional grade-control structures. *Journal of Hydraulic Engineering*, *138*(2), 167–176.

Sheppard, D. M., & Miller, W. (2006). Live-bed local pier scour experiments. *Journal of Hydraulic Engineering*, *132*(7), 635–642.

Wu, S., & Rajaratnam, N. (1996). Submerged flow regimes of rectangular sharp-crested weirs. *Journal of Hydraulic Engineering*, *122*(7), 412–414.

Wu, S., & Rajaratnam, N. (1998). Impinging jet and surface flow regimes at drop structures. *Journal of Hydraulic Research*, *36*(1), 69–74.

Yang, S. Q., Tan, S. K., & Lim, S. Y. (2005). Flow resistance and bed form geometry in a wide alluvial channel. *Water Resources Research*, *41*(9), W09419. doi:10.1029/2005wr004211